



Article

A Circulating Current Suppression Strategy for MMC Based on the $2N+1$ PWM Approach

Guozheng Zhang ¹, Jiahui Song ¹, Chen Li ² and Xin Gu ^{1,*}

¹ School of Electrical Engineering, Tiangong University, Tianjin 300387, China

² Advanced Electrical Equipment Innovation Center, Zhejiang University, Hangzhou 311107, China

* Correspondence: guxin@tiangong.edu.cn; Tel.: +86-1232-113-4212

Abstract: Compared with other topologies, the modular multilevel converter (MMC) has the advantages of higher scalability and lower harmonic distortion. When carrier-based pulse-width modulation approaches are used for the MMC, the number of carriers increases for more sub-modules, and the complexity of the control and the memory required increases as a result. In addition, the synchronization of several carriers is another issue. Due to the unique constructional characteristics of the MMC, circulating currents will be generated internally, causing distortions in the arm currents and, thus, unnecessary converter losses. In this paper, an improved $2N+1$ pulse-width modulation approach with low control complexity and a circulating current suppression strategy are proposed. Firstly, the conventional carrier phase-shifted $2N+1$ pulse-width modulation approach is improved so that the number of carrier signals adopted in each arm is always two. Secondly, the redundant switching states are used to suppress the circulating current. Finally, the effectiveness of the proposed strategy is verified experimentally. The results show that the proposed method reduces the control complexity while retaining the output performance. Meanwhile, the circulating current can be suppressed.

Keywords: modular multilevel converter (MMC); pulse-width modulation; circulating current



Citation: Zhang, G.; Song, J.; Li, C.; Gu, X. A Circulating Current Suppression Strategy for MMC Based on the $2N+1$ PWM Approach. *World Electr. Veh. J.* **2023**, *14*, 106. <https://doi.org/10.3390/wevj14040106>

Academic Editor: Joeri Van Mierlo

Received: 21 March 2023

Revised: 5 April 2023

Accepted: 10 April 2023

Published: 12 April 2023



Copyright: © 2023 by the authors. Licensee MDPI, Basel, Switzerland. This article is an open access article distributed under the terms and conditions of the Creative Commons Attribution (CC BY) license (<https://creativecommons.org/licenses/by/4.0/>).

1. Introduction

With the rapid development of electric transportation applications such as electric vehicles, electric vehicle charging stations, railway traction, and electric ships, the power converters adapted for them are attracting increasing attention. Multilevel converters for transportation are gaining wide acceptance owing to advantages such as improved waveform quality, reduced semiconductor losses, and low electromagnetic interference (EMI). As a new multilevel topology has emerged in recent years, the modular multilevel converter (MMC) has replaced the direct series connection of IGBT devices with a cascade of sub-modules and does not have the issues concerning dynamic voltage sharing of IGBT devices compared to conventional two-level converters and three-level converters. Compared to cascaded H-bridge converters, the MMC eliminates the use of multi-winding phase-shift transformers and can be extended to any voltage level and capacity by increasing the number of cascaded sub-modules. In addition, each sub-module can choose low-voltage power switching devices, with low switching frequency operation, which are easy to expand the use and significantly reduces the size, etc. However, the topology of this converter faces many challenges in terms of control operation and simulation modeling because of the unique operating principle [1,2].

As the most widely used modulation method for MMC, the carrier phase-shifted pulse-width modulation approach (CPSPWM) has advantages including balanced sub-module switching frequency, equal sub-module power distribution, and low harmonic distortion [3]. Meanwhile, MMC can generate two different types of output-phase voltage levels ($N+1$ and $2N+1$), according to the different arrangement of the carrier signals. The

carrier signal distribution method for the carrier phase-shifted $N+1$ pulse-width modulation and carrier phase-shifted $2N+1$ pulse width modulation is analyzed and compared in [4]. The results show that the output waveform quality of the carrier phase-shifted $2N+1$ pulse-width modulation approach is better. A generalized theory for the carrier phase-shifted modulation method for the MMC is proposed in [5], the output waveform quality is better when the number N of sub-modules in each arm is even. Due to internal calculation delays and the sampling mode, the complexity of carrier signal generation and the difficulty of accurate synchronization between the carrier signals increases significantly with the increase in sub-modules [6]. A single carrier-based alternative phase opposition disposition pulse-width modulation approach (APODPWM) was proposed in [7], which involves only simple mathematical calculations to solve the problem of accurately synchronizing multiple carrier signals. In [8], a single carrier based reconfigurable carrier-cascade modulation approach is proposed to make the output waveform satisfy both half-wave symmetry and quarter symmetry, and the experimental results show that the reconfigurable carrier-cascade modulation strategy reduces the total harmonic distortion of the output waveform compared with the conventional carrier modulation strategy. In [9], a dual carrier phase-shifted $N+1$ pulse-width modulation approach is proposed, in which multiple carrier signals are simplified according to mathematical methods. The complexity of the control algorithm is reduced, and the experimental results show that the output performance is the same as that of the conventional carrier phase-shifted modulation approach.

The different switched-in and switched-off states of the sub-modules cause inconsistent charging and discharging of the sub-module capacitors, which leads to large fluctuations in the capacitance of the sub-modules and generates corresponding circulating currents in each phase. The presence of the circulating current not only distorts the arm currents, but also increases the unnecessary loss of the converter. Circulating current suppression strategies can be divided into two categories, one for direct circulating current suppression strategies and the other for indirect circulating current suppression strategies. The phase leg contains two arms, and each arm contains N sub-modules, so the total of the voltage fluctuations at the AC ports of all the sub-modules of the two arms in the phase leg can be referred to as the voltage fluctuations of the phase leg. This fluctuating voltage is across the upper and lower arms and, therefore, generates fluctuating currents in the phase leg through the arm inductances. The fluctuating currents are defined as the circulating current [10]. The circulating current can be reduced by increasing the value of the arm inductance [11]. However, the circulating current cannot be completely eliminated. In [12–16], PI control under the second harmonic negative sequence coordinate system is used to control the second harmonic circulating current in the arm current. The control algorithm requires the second harmonic negative sequence coordinate transformation and feed-forward decoupling control, which increases the computational complexity of the control algorithm. In [17–19], the quasi-proportional resonant controller is used to track the circulating current in the arm current without static error, but each PR controller can only track the AC component of a specific frequency, which will lead to a more complex controller structure. To further reduce the system control complexity, a circulating current controller based on the $2N+1$ modulated redundant switching states is proposed in [20], which in turn achieves the effect of suppressing the capacitor voltage fluctuations. This circulating current controller avoids the problems of large computation and more complicated control parameter debugging that exist in traditional circulating current controllers (PI controller, PIR controller). A capacitor voltage fluctuation suppression strategy considering the arm inductance voltage was proposed in [21], which uses a new mathematical model considering the arm inductance voltage to obtain the reference signal for the circulating current and uses redundant switching states to control the circulating current. In [22], a circulating current suppression method based on capacitor voltage feed-forward compensation is proposed. The voltage fluctuations of the phase leg is used as the feed-forward compensation on the modulation signal to achieve the circulating current suppression. The additional circulating current controller is not needed. A circulating current suppression strategy without the arm current

sensor is proposed in [23]. It suppresses the circulating current by reducing the voltage fluctuations of the phase leg.

In order to reduce the control complexity and unnecessary losses of the MMC, an improved $2N+1$ pulse-width modulation approach and a circulating current suppression strategy are proposed in this paper. The number of carrier signals in each arm is reduced. The problem of accurate synchronization of multiple carrier signals can be solved. Meanwhile, this method utilizes the redundant switching states of the improved $2N+1$ PWM approach to suppress the circulating currents within the topology at the modulation level without the need for additional circulating current suppressors, and it is simple to implement.

The paper is organized as follows. Section 2 explains the basic operating principle of the MMC. Section 3 describes the development of the improved $2N+1$ pulse-width modulation approach. Section 4 depicts the circulating current suppression strategy based on the $2N+1$ modulated redundant switching states. Section 5 provides simulations and the experimental prototype results for the validation of the circulating current suppression strategy for the MMC based on the improved $2N+1$ pulse-width modulation approach. The article is concluded in Section 6.

2. MMC Operation Principle

The topology of the modular multilevel converter (MMC) is shown in Figure 1. The upper and lower arms of each phase are composed of N half bridge sub-modules and an arm inductance L_0 . V_{dc} is the DC-link voltage, v_x ($x \in \{A, B, C\}$) is the output-phase voltage, i_x is the output current. v_{xu} and v_{xl} are the voltage of the upper and lower arm, respectively. i_{xu} and i_{xl} are current of the upper and lower arm, respectively.

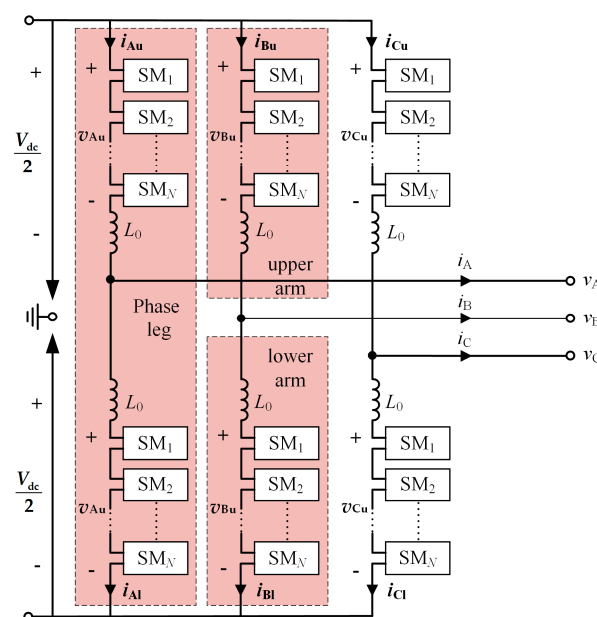


Figure 1. The topology of the modular multilevel converter (MMC).

As the most basic component of the MMC, the sub-modules have been derived from various types of structures. This paper is an example of a half bridge sub-module (HBSM), as shown in Figure 2. The sub-module topology is constructed from two IGBT power switching devices, T_1 and T_2 , with anti-parallel diodes and an energy storage capacitor. The MMC controls the turn-on and turn-off states of each half bridge sub-module power switching device in the upper and lower arms to obtain the required output voltage on the AC side. Each anti-parallel diode ensures that the corresponding IGBT power switching device can be protected from the current when it is turned off, thus ensuring that the MMC can operate normally. When T_1 is turned on and T_2 is turned off, the energy storage

capacitor will be charged or discharged according to the direction of the arm current flowing through it, when the sub-module is in the input state. When T_1 is off and T_2 is on, the output voltage of the sub-module is 0 V, and the arm current will not flow through the energy storage capacitor, at which time the sub-module is in the removal state. In addition, when both T_1 and T_2 are switched off, the sub-module will be in the removal state. When the arm current is positive, the capacitor is charged using the anti-parallel diode D_1 ; when the arm current is negative, the arm current will flow through the anti-parallel diode D_2 , and the capacitor will be bypassed. Table 1 shows the output voltage and switch state corresponding to the power switching device and defines the current direction of the arm current from end a to end b as the positive direction, v_{sm} is expressed as the output voltage of the sub-module unit and v_{cap} is the capacitance voltage of the sub-module.

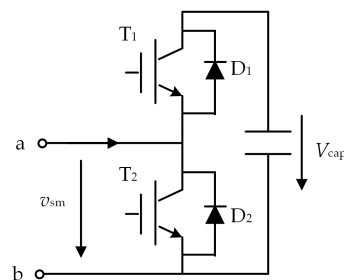


Figure 2. Half bridge sub-module topology.

Table 1. The output voltage and switch state corresponding to the power switching device.

| T_1 | T_2 | Arm Current Direction | Output Voltage | Working Status | Description |
|-------|-------|-----------------------|----------------|----------------|----------------------|
| ON | OFF | >0 | v_{cap} | Input state | Capacitive charging |
| ON | OFF | <0 | v_{cap} | Input state | Capacitive discharge |
| OFF | ON | >0 | 0 | Removal state | Capacitive bypass |
| OFF | ON | <0 | 0 | Removal state | Capacitive bypass |
| OFF | OFF | >0 | v_{cap} | Blocked state | Capacitive charging |
| OFF | OFF | <0 | 0 | Blocked state | Capacitive bypass |

The MMC equivalent mathematical model can reflect its operation principle visually, which is very important for the study of its operation control strategy. Firstly, in order to describe the equivalent mathematical model of the half bridge sub-module, S_{xki} can be defined as the switching function of the sub-module, as shown in Equation (1).

$$S_{xki} = \begin{cases} 1 & T_1 = 1, T_2 = 0 \\ 0 & T_1 = 0, T_2 = 1 \end{cases} \quad (1)$$

where, S_{xki} is the switching function of the i th half bridge sub-module of the k -arm in the x th phase ($k = u, l$), and when $S_{xki} = 1$, the corresponding half bridge sub-module is in the input state, and when $S_{xki} = 0$, the corresponding half bridge sub-module is in the removal state.

Since each half bridge sub-module is controlled individually, so that all half bridge sub-modules in the upper and lower arms can be equated to an independent controlled voltage source respectively, the output voltages, v_{xu} and v_{xl} , of the upper and lower arms in the x th phase unit can be expressed as:

$$\begin{cases} v_{xu} = \sum_{i=1}^N v_{sm_xui} = \sum_{i=1}^N S_{xui} v_{cap} \\ v_{xl} = \sum_{i=1}^N v_{sm_xli} = \sum_{i=1}^N S_{xli} v_{cap} \end{cases} \quad (2)$$

where, N is the total number of sub-modules of the arm, and v_{sm_xui} and v_{sm_xli} are the output voltages of the i th half bridge sub-module of the upper and lower arms of the x phase, respectively.

Because the three phase units of the MMC have the same structure and are controlled independently of each other, only a single phase needs to be analyzed. Taking phase A as an example, the single-phase equivalent circuit of the MMC is shown in Figure 3.

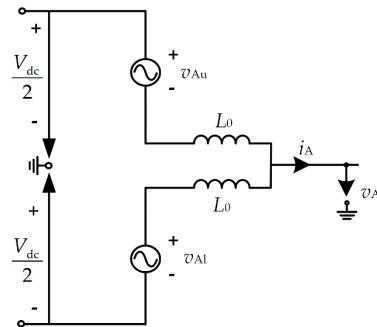


Figure 3. The single-phase equivalent circuit of the MMC.

The current flowing through the upper and lower arms is defined as the circulating current i_{cirA} . According to Kirchhoff's current law (KCL), the upper and lower arm currents can be expressed as:

$$\begin{cases} i_{Au} = i_{cirA} + \frac{i_A}{2} \\ i_{Al} = i_{cirA} - \frac{i_A}{2} \end{cases} \quad (3)$$

According to (1), the circulating current is derived as:

$$i_{cirA} = \frac{(i_{Au} + i_{Al})}{2} \quad (4)$$

The A-phase output voltage and output current are expressed as:

$$v_A = \sqrt{2}V_A \cos \omega t \quad (5)$$

$$i_A = \sqrt{2}I_A \cos(\omega t + \varphi) \quad (6)$$

where, V_A is the RMS value of the output-phase voltage, I_A is the RMS value of the output current, ω is the output fundamental angular frequency, and φ is the power factor angle.

According to the single-phase equivalent circuit of the MMC, the voltage equation of the upper and lower arms can be obtained by Kirchhoff's voltage law (KVL):

$$\begin{cases} \frac{V_{dc}}{2} - v_{Au} - L_0 \frac{di_{Au}}{dt} - v_A = 0 \\ \frac{V_{dc}}{2} - v_{Al} - L_0 \frac{di_{Al}}{dt} + v_A = 0 \end{cases} \quad (7)$$

To facilitate the analysis of the MMC, the voltage modulation index of phase A is defined as the ratio of the amplitude of the output AC-phase voltage to half the DC-side voltage:

$$m_A = \frac{\hat{V}_A}{\frac{1}{2}V_{dc}} = \frac{\sqrt{2}V_A}{\frac{1}{2}V_{dc}} = \frac{\sqrt{8}V_A}{V_{dc}} \quad (8)$$

where, \hat{V}_A is the amplitude of the output AC-phase voltage of phase A.

Ignoring the voltage drop in the arm inductance, the upper and lower arm voltage can be further expressed as:

$$\begin{cases} v_{Au} = \frac{V_{dc}}{2}(1 - m_A \cos \omega t) \\ v_{Al} = \frac{V_{dc}}{2}(1 + m_A \cos \omega t) \end{cases} \quad (9)$$

Substituting (3) with (7), it can be obtained that:

$$V_{dc} - (v_{Au} + v_{Al}) - 2L_0 \frac{di_{cirA}}{dt} = 0 \quad (10)$$

$$\frac{(v_{Al} - v_{Au})}{2} - \frac{L_0}{2} \frac{di_A}{dt} - v_A = 0 \quad (11)$$

In order to more directly describe the energy exchange process inside the MMC and the relationship between each electrical quantity, the equivalent circuit of phase A can be decomposed into the DC-side equivalent circuit and the AC-side equivalent circuit, as shown in Figure 4a,b. Figure 4a depicts the energy exchange process between the MMC and the DC side, which reflects the correlation between each electrical quantity within the topology, so that the MMC can indirectly control the circulating current to achieve a specific goal using Equation (10). Equation (11) and Figure 4b both describe the process of energy interaction between the MMC and the AC side, which reflects that the MMC can get the required output voltage on the AC side by controlling the opening and closing states of each half bridge sub-module power switching device in the upper and lower arms.

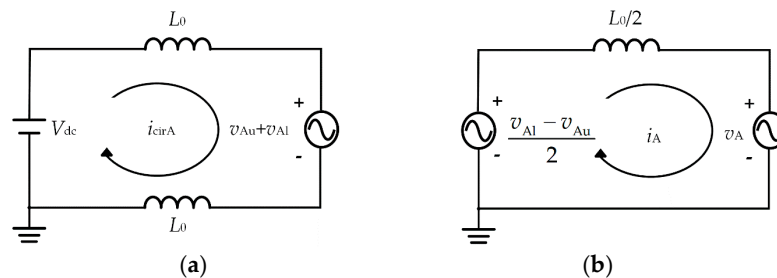


Figure 4. The equivalent circuit of phase A. (a) DC-side equivalent circuit, (b) AC-side equivalent circuit.

3. Improved 2N+1 Pulse-Width Modulation Approach

The control strategy can rely on the pulse-width modulation approach to generate pulses to control the MMC and, thus, improve the system performance. The carrier-based pulse-width modulation approach is often used in the MMC because of its simplicity, scalability and good control performance. Compared with other converters, the MMC can generate two different types of output-phase voltage levels, $N+1$ and $2N+1$, depending on the different arrangements of the multiple carrier signals in the upper and lower arms and the parity of the number of sub-modules in the arm. Figure 5 shows the principle of the conventional carrier phase-shifted $2N+1$ pulse-width modulation approach under the $N = 4$ condition. Each arm requires a modulation signal and a set of four carrier signals with the frequency of f_c and the phase difference of $\pi/2$. At the same time, since the upper and lower arms in the MMC phase cell operate symmetrically, the phases of the modulated signals of the upper and lower arms need to differ from each other by π . The carrier signals of the upper arm are defined as $C_{p1} \sim C_{p4}$, and the carrier signals of the lower arm are defined as $C_{n1} \sim C_{n4}$. Taking C_{p1} and C_{n1} as an example, the phase shifting angle θ between the carrier signals of the upper and lower arm is $\pi/4$.

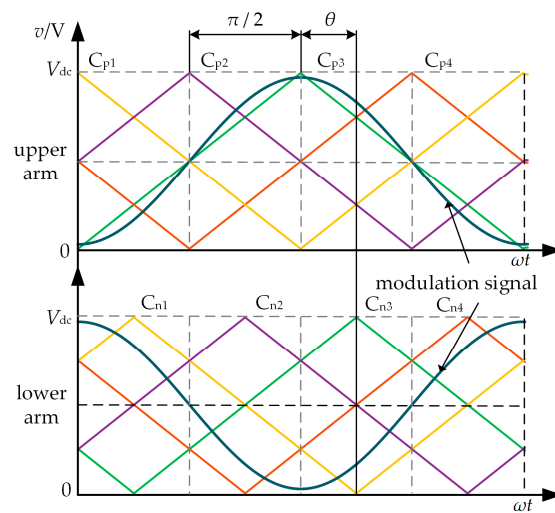


Figure 5. The principle of the conventional carrier phase-shifted $2N+1$ pulse-width modulation approach ($N = 4$).

With the increase in sub-modules in each arm, the number of carrier signals is increased correspondingly. Moreover, the accurate synchronization of the different carrier signals will be more difficult. In order to solve the above problem, an improved $2N+1$ pulse-width modulation approach is proposed. Only two carrier signals are used to generate $2N+1$ level output-phase voltage. Taking $N = 4$ as an example, the principle of the improved $2N+1$ pulse-width modulation approach is shown in Figure 6. The fundamental period is divided into four segments, and the carrier wave is divided into two zones, according to its amplitude. There are only two carrier signals with a phase difference of π in any arbitrary rectangle determined by the segment number and zone number.

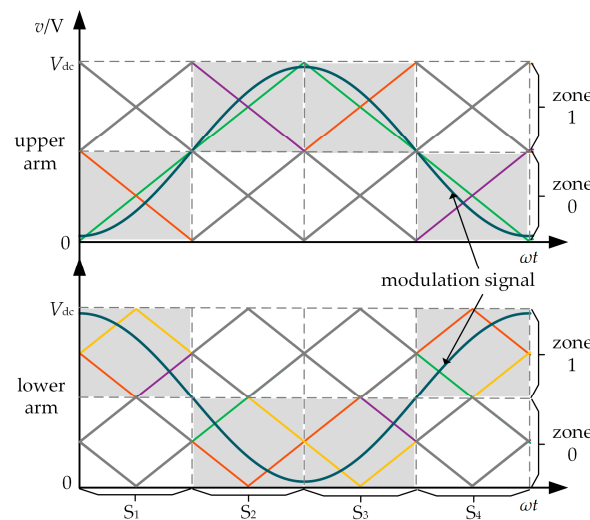


Figure 6. The principle of the improved $2N+1$ pulse-width modulation approach ($N = 4$).

Figure 7 shows the block diagram of the improved modulation method. The implementation of the proposed method can be divided into three steps: the generation of the segment and zone number, the integration of the modulation signal, and the comparison of the modulation signal and the carrier signal. In each segment, the modulation signal is vertically shifted to zone 0, to generate an integrated modulation signal, as shown in Figure 8. Only two carrier signals with a phase difference of π are adopted in each arm, as shown in Figure 9. The carrier signal of the lower arm is shifted by $\pi/2$ with respect to the upper arm (the phase difference between carrier 1 and carrier 2 is π , the phase difference

between carrier 1 and carrier 3 is $\pi/2$, and the phase difference between carrier 2 and carrier 4 is also $\pi/2$). The carrier signals set on the upper and lower arms are compared with the corresponding modulated wave integration signals, respectively. The carrier signals are compared with the corresponding integrated modulation signals of the upper and lower arms, respectively. Finally, the comparison results are superposed with the segment and zone number to generate the number of sub-modules needed to be switched in for the upper and lower arms. Then, the driving pulse of each sub-module is generated.

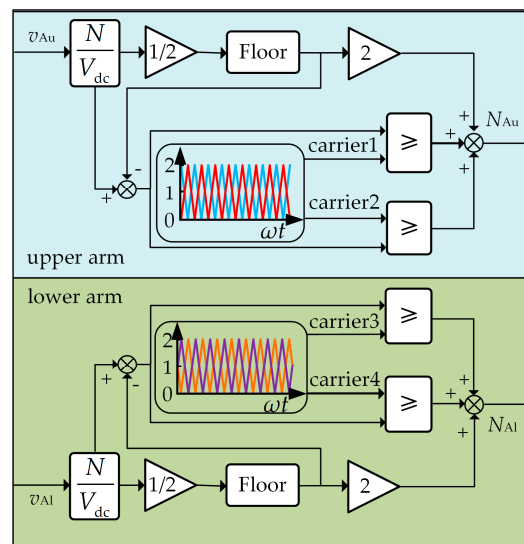


Figure 7. The block diagram of the improved modulation method.

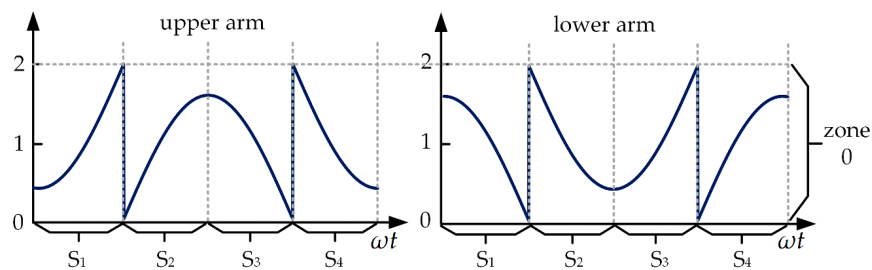


Figure 8. The integrated modulation signals.

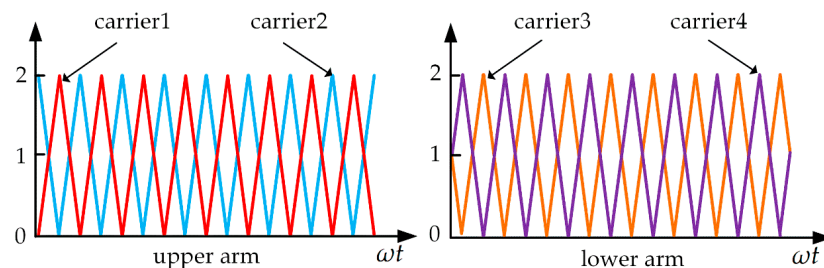


Figure 9. The carrier signals.

4. Circulating Current Suppression Strategy

For the three-phase MMC with N sub-modules in each arm, the phase voltage will appear at the $N+1$ voltage level if the total number of switched-in sub-modules in each phase remains N . If the total number of switched-in sub-modules changes among $N-1$, N , and $N+1$, the phase voltage will appear at the $2N+1$ voltage level. Taking $N = 4$ as an example, the output-phase voltage of the $2N+1$ modulation method is shown in Figure 10.

The relationship between the total number of switched-in sub-modules and the output-phase voltage level is shown in Table 2. It follows that the switching states generated by its $2N+1$ modulation strategy consist of non-redundant switching states and redundant switching states. When the number of phase voltage levels on the output side of the MMC system is 0, 2, 4, 6, or 8 even levels, only one switch state type can generate that phase voltage level and a total of four sub-modules are put into the phase arm. When the number of phase voltage levels on the output side of the MMC system is 1, 3, 5, or 7 odd levels, there are two switching state types to generate that phase voltage level and a total of three or four sub-modules are put into the phase arm. Therefore, for the even output voltage level, N sub-modules are switched in for each phase. While for the odd output voltage level, the $N+1$ or $N-1$ sub-modules are switched in for each phase. Thus, there is only one switching state corresponding to even output voltage level and there are two switching states corresponding to the odd output voltage level. The DC-side equivalent circuit of the MMC is shown in Figure 11. The circulating current will increase if the $N-1$ sub-modules are switched in. The circulating current will decrease if the $N+1$ sub-modules are switched in. Thus, the circulating current can be controlled by the above two switching states.

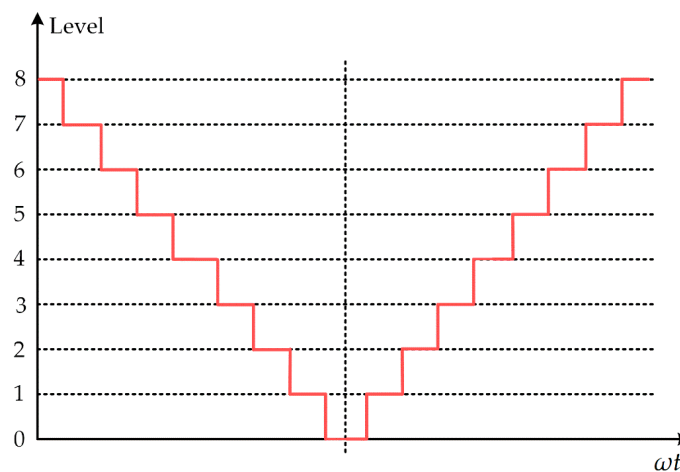


Figure 10. The output-phase voltage of the $2N+1$ modulation method.

Table 2. The relationship between the total number of switched-in sub-modules and the output-phase voltage level.

| Phase Voltage Level | Input of Sub-Module Number of Upper Arm | Input of Sub-Module Number of Lower Arm | Input of Sub-Module Number of Phase Leg |
|---------------------|---|---|---|
| 0 | 4 | 0 | 4 |
| 1 | 4 3 | 1 0 | 5 3 |
| 2 | 3 | 1 | 4 |
| 3 | 3 2 | 2 1 | 5 3 |
| 4 | 2 | 2 | 4 |
| 5 | 2 0 | 3 3 | 5 3 |
| 6 | 1 | 3 | 4 |
| 7 | 1 0 | 4 3 | 5 3 |
| 8 | 0 | 4 | 4 |

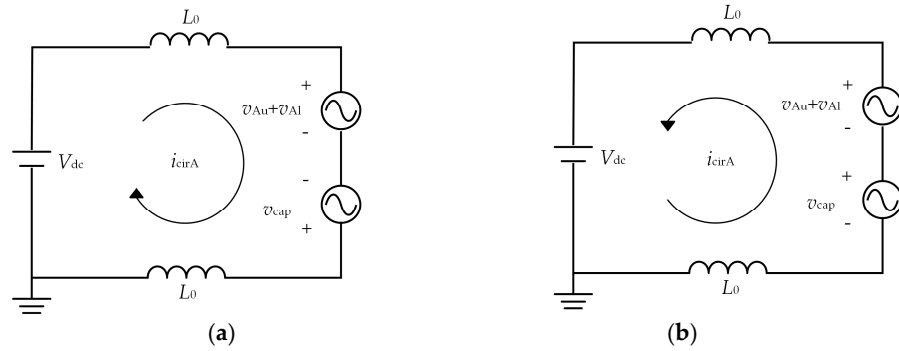


Figure 11. The DC-side equivalent circuit of the MMC. (a) $N-1$ sub-modules are switched in for phase A, (b) $N+1$ sub-modules are switched in for phase A.

The instantaneous power of the upper and lower arms can be expressed as:

$$p_{Au} = -\frac{\sqrt{2}m_A V_{dc} I_A}{8} \cos \varphi + \frac{\sqrt{2}V_{dc} I_A}{4} \cos(\omega t + \varphi) - \frac{\sqrt{2}m_A V_{dc} I_A}{8} \cos(2\omega t + \varphi) + \frac{V_{dc}}{2} i_{cirA} - \frac{m_A V_{dc}}{2} i_{cirA} \cos(\omega t) \quad (12)$$

$$p_{Al} = -\frac{\sqrt{2}m_A V_{dc} I_A}{8} \cos \varphi - \frac{\sqrt{2}V_{dc} I_A}{4} \cos(\omega t + \varphi) - \frac{\sqrt{2}m_A V_{dc} I_A}{8} \cos(2\omega t + \varphi) + \frac{V_{dc}}{2} i_{cirA} + \frac{m_A V_{dc}}{2} i_{cirA} \cos(\omega t) \quad (13)$$

For MMC, the circulating current only contains even order harmonic components. Moreover, the second order harmonic component accounts for a large proportion [24]. The circulating current can also be expressed as:

$$i_{cirA} = I_{cirA_dc} + \sqrt{2}I_{cirA_2} \cos(2\omega t + \theta) \quad (14)$$

where I_{cirA_dc} is the DC component of the circulating current, and I_{cirA_2} and θ are the RMS value and the phase of the second order harmonic component of the circulating current, respectively.

In order to suppress the circulating current, the reference value of the circulating current can be set to the value of the DC component. Meanwhile, to ensure the power balance between the DC side and the AC side of the MMC, the DC component of the instantaneous power of the arm should be kept at zero [25]. Therefore, the reference value $i_{cirA_suppressing}^*$ of the circulating current can be derived as:

$$i_{cirA_suppressing}^* = \frac{\sqrt{2}m_A I_A}{4} \cos \varphi \quad (15)$$

Taking the A-phase as an example, the block diagram of the circulating current suppression strategy based on the improved $2N+1$ pulse-width modulation approach is shown in Figure 12. Based on the modulation signals of the upper and lower arms, the number of sub-modules that need to be switched in is determined by the improved carrier phase-shifted $2N+1$ modulation method. The circulating current can be adjusted to its reference value $i_{cirA_sum}^*$ by the redundant switching state ($N+1$ or $N-1$ sub-modules are switched in). $i_{cirA_sum}^*$ consists of a reference component $i_{cirA_balance}^*$ generated by the MMC internal energy balance control [26] and a reference component $i_{cirA_suppressing}^*$ aimed at suppressing the circulating current. That is, when the voltage level is at the redundant level and $i_{cirA} \leq i_{cirA_sum}^*$, the $N-1$ sub-modules are selected to be put into the phase, so that the circulating current inside the topology rises; conversely, when the voltage level is at the redundant voltage level and $i_{cirA} > i_{cirA_sum}^*$, the $N+1$ sub-modules are selected to be put into the phase, so that the circulating current inside the topology falls and, finally, after

the capacitor voltage sequencing algorithm, the trigger pulse is applied to the modular multilevel converter. In particular, the capacitor voltage sorting algorithm [27] in this block diagram, the most widely used method for balancing the capacitive voltage of sub-modules, determines the specific sub-modules to be put into the bridge arm by sorting the capacitive voltage of all sub-modules in the arm and determining the number of sub-modules to be put into the arm at the present time, as well as the direction of the arm current. The purpose of this is that when the arm current is positive, the sub-module with the lower capacitor voltage is engaged for a longer period of time to charge the capacitor, while when the arm current is negative, the sub-module with the higher capacitor voltage is engaged for a longer period of time to discharge the capacitor.

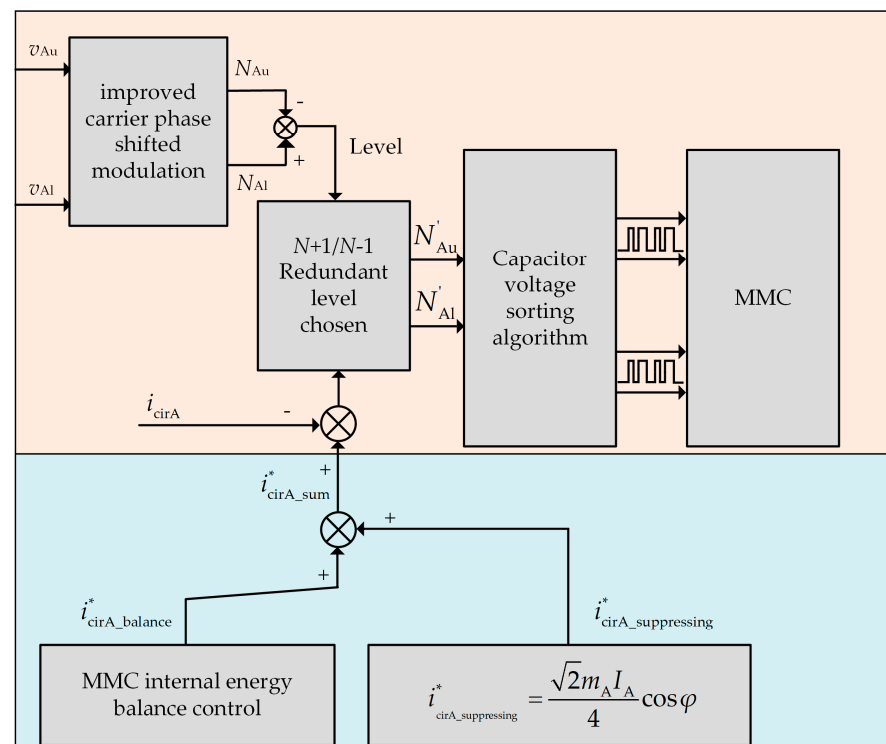


Figure 12. The block diagram of the circulating current suppression strategy based on the improved 2N+1 pulse-width modulation approach.

5. Experimental Verification

To verify the performance of the circulating current suppression strategy of the MMC based on the improved 2N+1 pulse-width modulation approach, the simulation models of the three-phase MMC system were developed in MATLAB/Simulink. In addition, the experimental prototype of the three-phase MMC system was designed and developed in the laboratory. The Canadian Opal-RT[®] rapid prototyping system OP5700 was adopted as the controller and the Switzerland Imperix[®] PEH2015 power electronic building block was used to compose the MMC ($N = 4$), as shown in Figure 13. The load condition was set as a simple resistor–inductor (R–L) (resistor–inductor) load. Based on the instantaneous power of the upper and lower arms, it is known that the control performance of the MMC depends on the power factor and, therefore, the simulations and experiments with the proposed 2N+1 pulse-width modulation method and the conventional carrier phase-shifted 2N+1 pulse-width modulation method are carried out under different load power factor conditions. The parameters for the simulations and experiments are shown in Table 3.

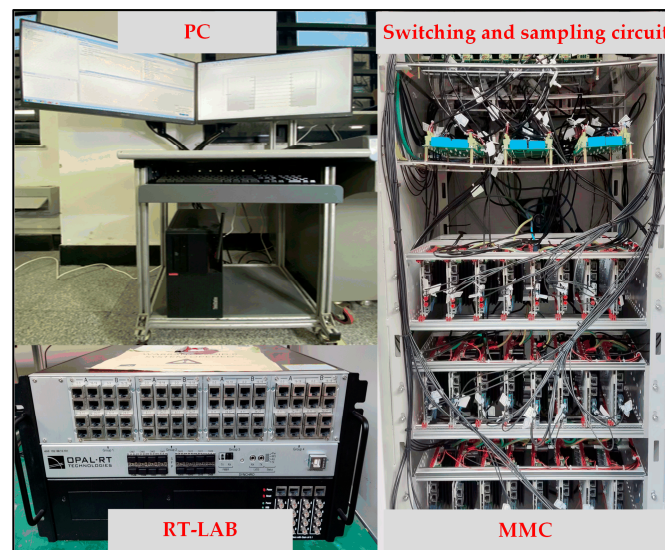


Figure 13. The prototype of the Opal-RT® OP5700 driven MMC.

Table 3. The simulation and experimental parameters.

| Parameters | Simulation | Experiment |
|-------------------------------|-------------|-------------|
| DC-side voltage V_{dc}/V | 800 | 200 |
| Number of SMs per arm N | 8 | 4 |
| Sub-module capacitance C/mF | 5.04 | 5.04 |
| Arm inductance L_0/mH | 2 | 1 |
| Load resistance R/Ω | 5 | 5 |
| Load inductance L/mH | 5/20 | 5/20 |
| Rated frequency f/Hz | 50 | 50 |
| Carrier frequency f_c/kHz | 2 | 2 |
| Voltage modulation index m | 0.9 | 0.8 |
| Load power factor $\cos\phi$ | 0.954/0.623 | 0.954/0.623 |

To demonstrate the simplicity of the implementation of the proposed $2N+1$ pulse-width modulation method, the MMC simulations were developed using the parameters for simulation in Table 3. When the arm is used with eight sub-modules, the proposed method requires only two differently phased carriers compared to the conventional carrier phase-shifted modulation method, which requires eight differently phased carriers, thus the control complexity of the system is reduced.

The circulating current, i_{cirA} , of the proposed method and the conventional method under different load power factor conditions are shown in Figures 14 and 15. For $\cos\phi = 0.954$, the simulated ripples of the circulating current are 8.1 A and 41 A for the proposed method and the conventional method, respectively. For $\cos\phi = 0.623$, the simulated ripples of the circulating current are 6.2 A and 16.5 A for the proposed method and the conventional method, respectively. It is clear that the proposed method can suppress the circulating current effectively.

The output line voltage v_{AB} , the output-phase voltage v_A , and the output current i_A of the proposed method and the conventional method under different load power factor conditions are shown in Figures 16 and 17. As the arm contains eight sub-modules, the number of levels in the output-phase voltage waveform under the $2N+1$ modulation is 17 levels for $m = 0.9$. If the total harmonic distortion rate of the output current is used as the evaluation standard for the MMC output waveform, the total harmonic distortion of the output current I_{THD} for the proposed method and the conventional method under different load power factor conditions are shown in Figures 18 and 19. The I_{THD} of the proposed and the conventional methods are approximately the same. This demonstrates the similarity in the output performance between the proposed modulation method and the conventional modulation method.

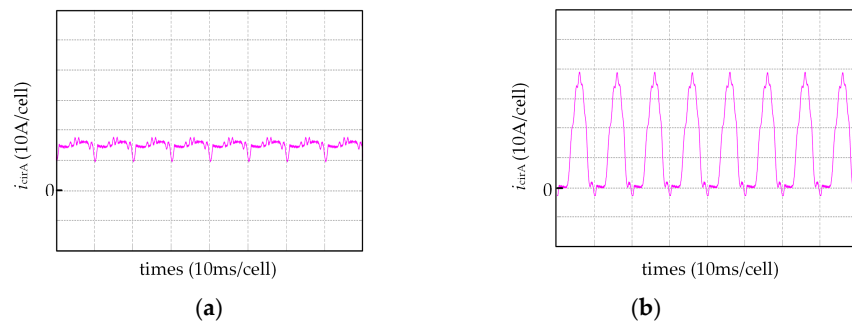


Figure 14. Simulated waveform of the circulating current fluctuation at $\cos\phi = 0.954$ ($N = 8$). (a) The proposed modulation method, (b) the conventional modulation method.

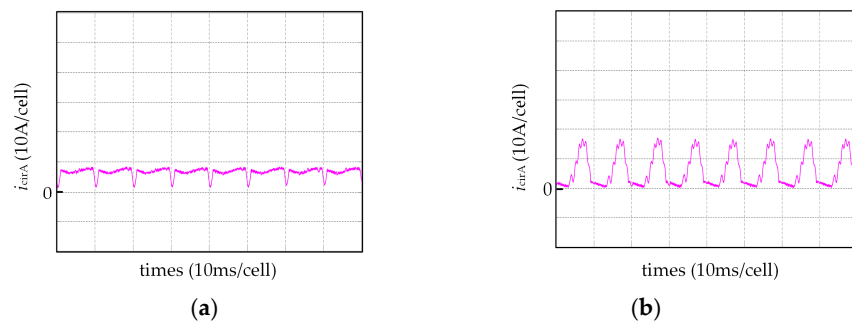


Figure 15. Simulated waveform of the circulating current fluctuation at $\cos\phi = 0.623$ ($N = 8$). (a) The proposed modulation method, (b) the conventional modulation method.

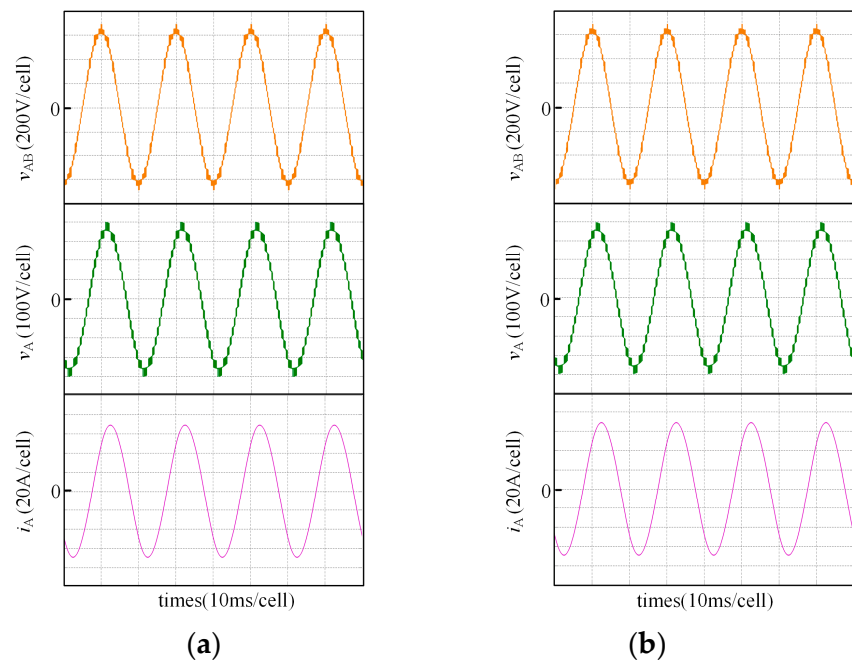


Figure 16. Experimental output waveforms of the converter at $\cos\phi = 0.954$ ($N = 8$). (a) The proposed modulation method, (b) the conventional modulation method.

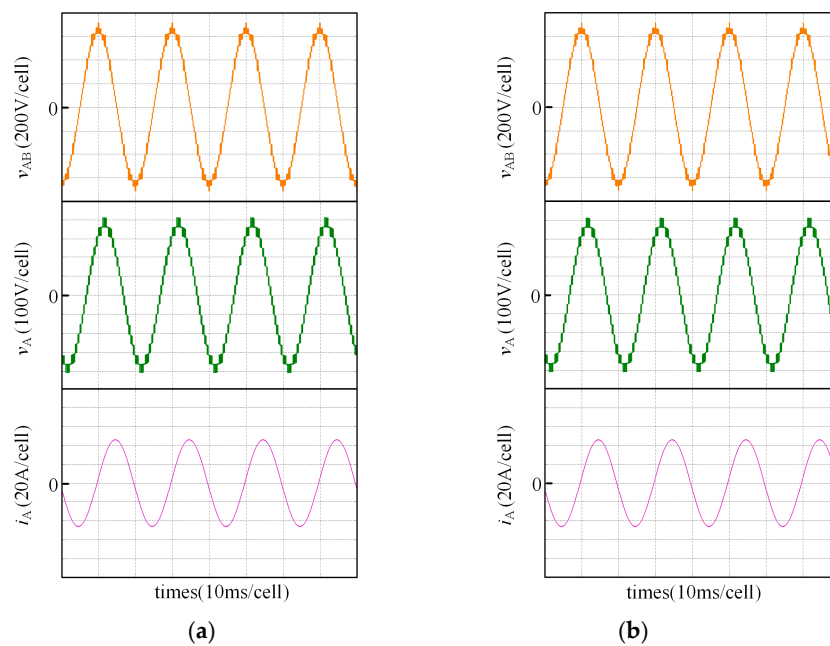


Figure 17. Experimental output waveforms of the converter at $\cos\phi = 0.623$ ($N = 8$). (a) The proposed modulation method, (b) the conventional modulation method.

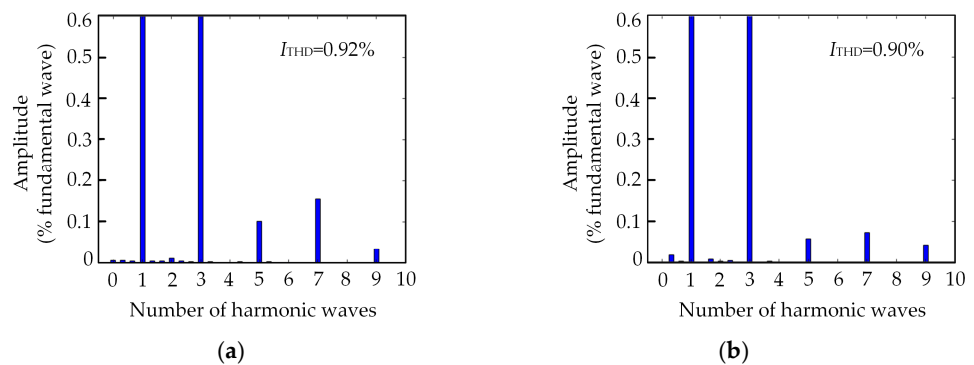


Figure 18. The total harmonic distortion of the output current at $\cos\phi = 0.954$ ($N = 8$). (a) The proposed modulation approach, (b) the conventional modulation approach.

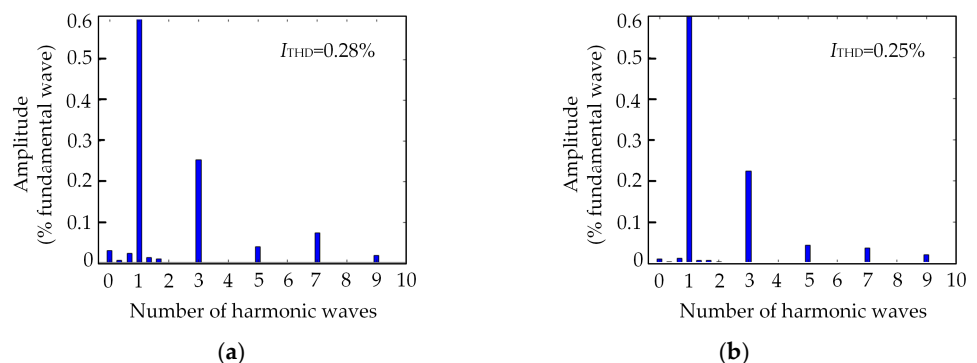


Figure 19. The total harmonic distortion of the output current at $\cos\phi = 0.623$ ($N = 8$). (a) The proposed modulation approach, (b) the conventional modulation approach.

Furthermore, the proposed method was verified through the experimental prototype of the three-phase MMC system. The circulating current i_{cirA} of the proposed method and the conventional method under different load power factor conditions are shown in Figures 20 and 21. For $\cos\phi = 0.954$, the ripples of the circulating current are 3.8 A and

5.8 A for the proposed method and the conventional method, respectively. For $\cos\varphi = 0.623$, the ripples of the circulating current are 3.4 A and 4.4 A for the proposed method and the conventional method, respectively. It is obvious that the proposed method uses redundant switching states with the $2N+1$ modulation to regulate the circulating current of the MMC with its reference value in order to achieve the effect of suppressing the circulating current fluctuations at different load power factors.

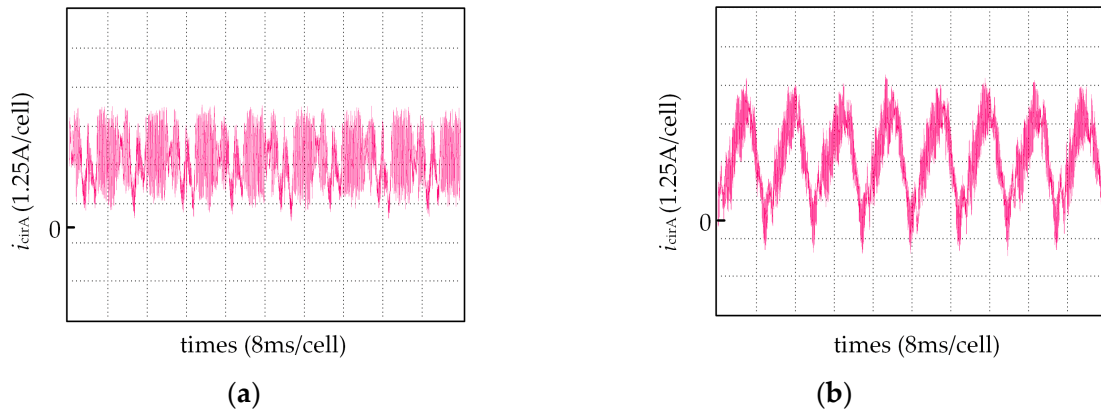


Figure 20. Experimental waveform of the circulating current fluctuation at $\cos\varphi = 0.954$ ($N = 4$). (a) The proposed modulation method, (b) the conventional modulation method.

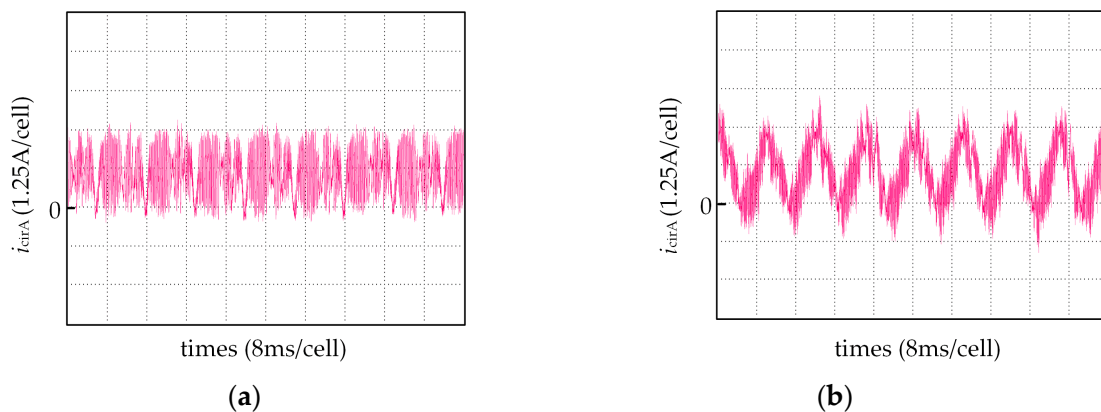


Figure 21. Experimental waveform of the circulating current fluctuation at $\cos\varphi = 0.623$ ($N = 4$). (a) The proposed modulation method, (b) the conventional modulation method.

To demonstrate the similarity between the proposed modulation method and the conventional modulation method, the experimental output waveforms of the two methods for different power factor conditions are shown in Figures 22 and 23. As can be seen, for $m = 0.8$, the output-phase voltage of the carrier phase-shifted $2N+1$ modulation method has nine voltage levels. Thus, the output current is an undistorted sinusoidal waveform. For different load power factors, the I_{THD} of the proposed and the conventional methods are approximately the same, as shown in Figures 24 and 25. This proves that the proposed modulation method presents an identical performance to the conventional modulation method. Thus, the proposed method not only reduces the circulating current, but also ensures the quality of the output waveform, the advantages of which are shown in Tables 4 and 5.

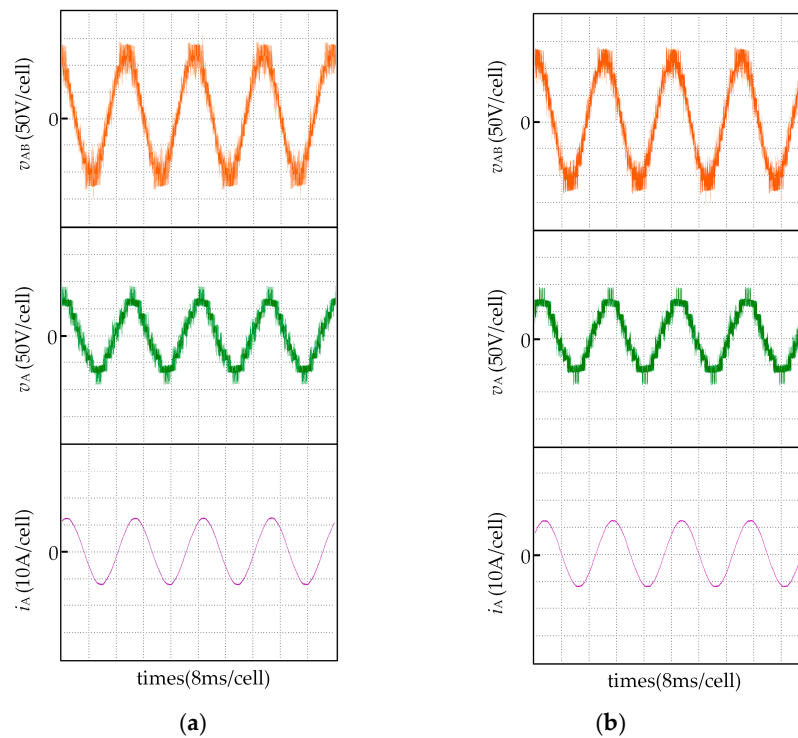


Figure 22. Experimental output waveforms of the converter at $\cos\varphi = 0.954$ ($N = 4$). (a) The proposed modulation method, (b) the conventional modulation method.

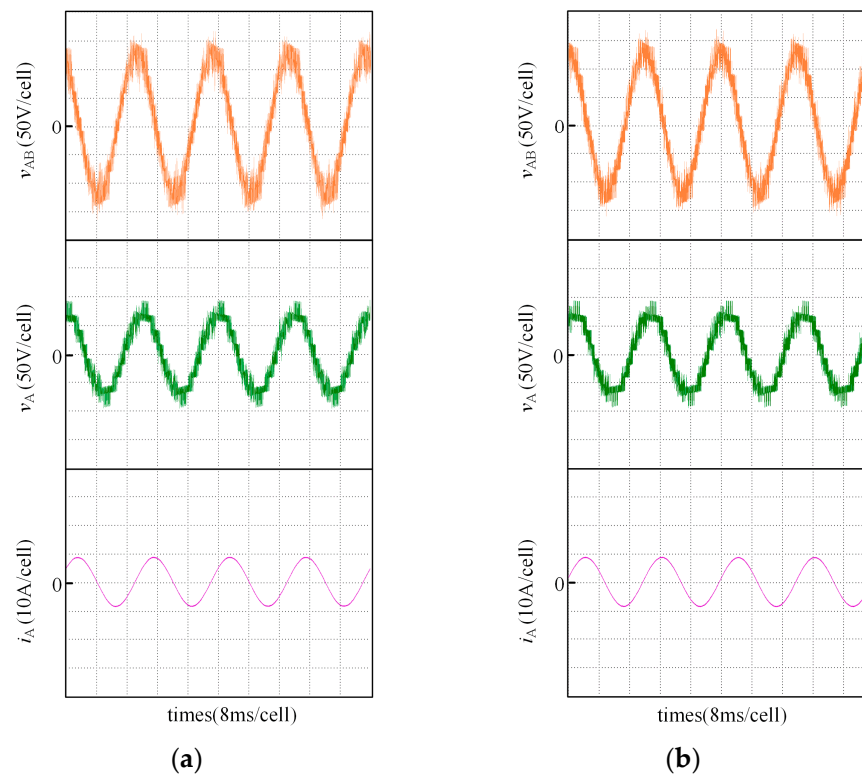


Figure 23. Experimental output waveforms of the converter at $\cos\varphi = 0.623$ ($N = 4$). (a) The proposed modulation method, (b) the conventional modulation method.

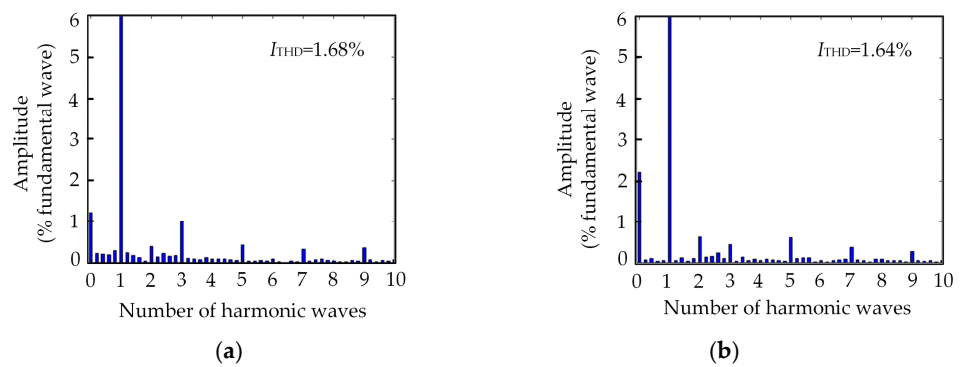


Figure 24. The total harmonic distortion of the output current at $\cos\varphi = 0.954$ ($N = 4$). (a) The proposed modulation approach, (b) the conventional modulation approach.

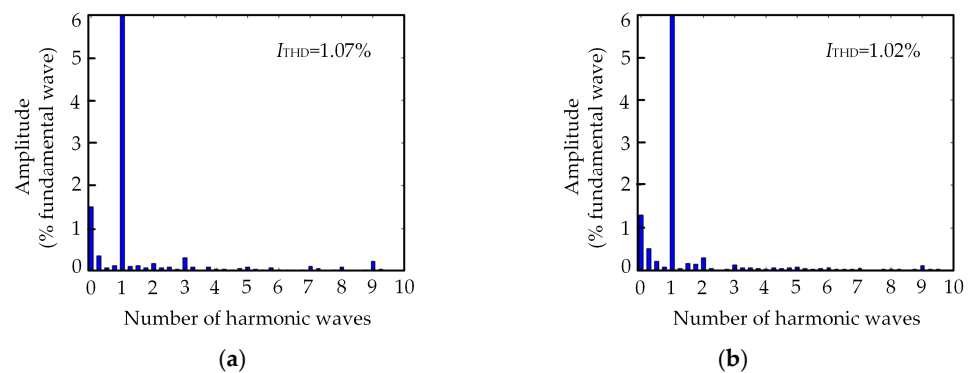


Figure 25. The total harmonic distortion of the output current at $\cos\varphi = 0.623$ ($N = 4$). (a) The proposed modulation approach, (b) the conventional modulation approach.

Table 4. Features of the different approaches at $\cos\varphi = 0.954$.

| Features | Simulation ($N = 8$) | | Experiment ($N = 4$) | |
|---------------------------------|------------------------|---------------------------|------------------------|---------------------------|
| | The Proposed Approach | The Conventional Approach | The Proposed Approach | The Conventional Approach |
| Number of carriers per arm | 2 | 8 | 2 | 4 |
| Circulating current fluctuation | 8.1 A | 41 A | 3.8 A | 5.8 A |
| I_{THD} | 0.92% | 0.90% | 1.68% | 1.64% |

Table 5. Features of the different approaches at $\cos\varphi = 0.623$.

| Features | Simulation ($N = 8$) | | Experiment ($N = 4$) | |
|---------------------------------|------------------------|---------------------------|------------------------|---------------------------|
| | The Proposed Approach | The Conventional Approach | The Proposed Approach | The Conventional Approach |
| Number of carriers per arm | 2 | 8 | 2 | 4 |
| Circulating current fluctuation | 6.2 A | 16.5 A | 3.4 A | 4.4 A |
| I_{THD} | 0.28% | 0.25% | 1.07% | 1.02% |

6. Conclusions

This paper discusses and investigates carrier-based pulse-width modulation methods and circulating current suppression strategies for MMC applications, and proposes an improved $2N+1$ pulse-width modulation approach with circulating current suppression.

First of all, the improved $2N+1$ pulse-width modulation approach allows the number of carrier signals to be decoupled from the number of sub-modules in the arm, in other words, for any number of sub-modules, the number of carrier signals used in each arm is always two. Secondly, the circulating current is controlled by different redundant switching states of the $2N+1$ pulse-width modulation approach, eliminating the need for an additional circulating current controller. Compared with the conventional method, the complexity of the proposed method is reduced. At the same time, the improved approach also has some limitations, such as this approach cannot be controlled independently for each sub-module, and must be combined with the capacitor voltage sequencing algorithm to achieve uniform power distribution among the sub-modules and to suppress the purpose of the circulating current. Finally, the effectiveness of the proposed method is verified through simulations and experimental prototypes on RT-Lab under different working conditions. The simulation and experimental results show that the proposed method not only suppresses the circulating currents effectively, but also preserves the output waveform quality of the carrier phase-shifted $2N+1$ pulse-width modulation approach.

Author Contributions: Conceptualization, G.Z. and X.G.; methodology, J.S. and G.Z.; software, J.S.; validation, J.S.; formal analysis, J.S. and C.L.; writing—original draft preparation, J.S.; writing—review and editing, X.G. and G.Z.; funding acquisition, X.G. All authors have read and agreed to the published version of the manuscript.

Funding: This research was funded by “The National Natural Science Foundation of China, grant number 52177055”, “The Zhejiang Provincial Basic Public Welfare Research Projects, grant number LGG22E070010”.

Data Availability Statement: Not applicable.

Conflicts of Interest: The authors declare no conflict of interest.

Nomenclature

| | |
|-------------|---|
| MMC | Modular multilevel converter |
| CPSPWM | Carrier phase-shifted pulse-width modulation |
| APODPWM | Alternative phase opposition disposition pulse-width modulation |
| HBSM | Half bridge sub-module |
| L_0 | Arm inductance |
| V_{dc} | DC-link voltage |
| v_x | Output-phase voltage ($x \in \{A, B, C\}$) |
| i_x | Output current |
| v_{xu} | Voltage of upper arm |
| v_{xl} | Voltage of lower arm |
| i_{xu} | Current of upper arm |
| i_{xl} | Current of lower arm |
| v_{sm} | Output voltage of the sub-module |
| v_{cap} | Capacitance voltage of the sub-module |
| N | The total number of sub-modules in the arm |
| V_A | The RMS value of A-phase output-phase voltage |
| I_A | The RMS value of A-phase output current |
| v_{AB} | The output line voltage of phase A and B |
| \hat{V}_A | Amplitude of A-phase output-phase voltage |
| m | Voltage modulation index |
| KVL | Kirchhoff's voltage law |

References

1. Dekka, A.; Wu, B.; Fuentes, R.L. Evolution of Topologies, Modeling, Control Schemes, and Applications of Modular Multilevel Converters. *IEEE J. Emerg. Sel. Top. Power Electron.* **2017**, *5*, 1634–1656. [[CrossRef](#)]
2. Debnath, S.; Qin, J.; Bahrani, B. Operation, Control, and Applications of the Modular Multilevel Converter: A Review. *IEEE Trans. Power Electron.* **2015**, *30*, 37–53. [[CrossRef](#)]

3. Li, B.; Yang, R.; Xu, D. Analysis of the Phase-Shifted Carrier Modulation for Modular Multilevel Converters. *IEEE Trans. Power Electron.* **2014**, *30*, 297–310. [[CrossRef](#)]
4. Bekhouche, R.; Khoucha, F.; Benrabah, A. Comparison of PWM Techniques for Modular Multilevel Converter: A Comparison Based on Different Voltage Level Waveforms. In Proceedings of the 2020-1st International Conference on Communications, Control Systems and Signal Processing (CCSSP), El Oued, Algeria, 16–17 May 2020; pp. 460–465.
5. Ronanki, D.; Williamson, S.S. A Novel $2N+1$ Carrier-Based Pulse Width Modulation Scheme for Modular Multilevel Converters with Reduced Control Complexity. In Proceedings of the 2019 IEEE Applied Power Electronics Conference and Exposition (APEC), Anaheim, CA, USA, 17–21 March 2019; pp. 908–915.
6. Ghias, A.; Pou, J.; Capela, G. Single-Carrier Phase-Disposition PWM Implementation for Multilevel Flying Capacitor Converters. *IEEE Trans. Power Electron.* **2015**, *30*, 5376–5380. [[CrossRef](#)]
7. Li, Y.; Wang, Y.; Li, B.Q. Generalized Theory of Phase-Shifted Carrier PWM for Cascaded H-Bridge Converters and Modular Multilevel Converters. *IEEE J. Emerg. Sel. Top. Power Electron.* **2016**, *4*, 589–605. [[CrossRef](#)]
8. Muthavarapu, A.K.; Anjana, K.G.; Biswas, J. A reconfigurable integrated level shifted carrier based PWM method for modular multilevel converters. *IEEE Trans. Electr. Electron. Eng.* **2022**, *17*, 1148–1159. [[CrossRef](#)]
9. Alikhani, M.; Khaburi, D.A.; Khosravi, M. PSC-PWM Scheme for Modular Multilevel Converters with Highly-reduced Carrier Numbers and Low Control Complexity. In Proceedings of the 2022-13th Power Electronics, Drive Systems, and Technologies Conference (PEDSTC), Tehran, Iran, 1–3 February 2022; pp. 660–664.
10. Li, X.; Song, Q.; Liu, W. Performance Analysis and Optimization of Circulating Current Control for Modular Multilevel Converter. *IEEE Tran. Ind. Electron.* **2016**, *63*, 716–727. [[CrossRef](#)]
11. Li, Y.; Jones, E.A.; Wang, F. Circulating Current Suppressing Control's Impact on Arm Inductance Selection for Modular Multilevel Converter. *IEEE J. Emerg. Sel. Top. Power Electron.* **2016**, *5*, 182–188. [[CrossRef](#)]
12. Tu, Q.; Zheng, X.; Jing, Z. Circulating current suppressing controller in modular multilevel converter. In Proceedings of the 2010-36th Annual Conference on IEEE Industrial Electronics Society, Glendale, AZ, USA, 7–10 November 2010; pp. 3198–3202.
13. Tu, Q.; Xu, Z.; Xu, L. Reduced Switching-Frequency Modulation and Circulating Current Suppression for Modular Multilevel Converters. *IEEE Trans. Power Deliv.* **2011**, *26*, 2009–2017.
14. Reddy, G.A.; Shukla, A. Optimized Circulating Current Injection Control Scheme for Modular Multilevel Converters. In Proceedings of the 2021 IEEE Energy Conversion Congress and Exposition (ECCE), Vancouver, BC, Canada, 10–14 October 2021; pp. 2444–2450.
15. Yang, Z.; Song, P.; Song, J. An MMC Circulating Current Suppressing Controller Based on Arm Common-Mode Voltage. *IEEE Access* **2020**, *8*, 189471–189478. [[CrossRef](#)]
16. Yang, Z.; Zhang, K.; Li, X. A Control Strategy for Suppressing Submodule Capacitor Voltage Fluctuation of MMC Based on Circulating Current Voltage Drop Balance. *IEEE Access* **2021**, *9*, 9130–9141. [[CrossRef](#)]
17. Wang, J.; Han, X.; Ma, H. Analysis and Injection Control of Circulating Current for Modular Multilevel Converters. *IEEE Trans. Ind. Electron.* **2019**, *66*, 2280–2290. [[CrossRef](#)]
18. Alharbi, M.; Isik, S.; Bhattacharya, S. Control of Circulating Current to Minimize the Rating of the Energy Storage Device in Modular Multilevel Converters. In Proceedings of the 2019 IEEE Energy Conversion Congress and Exposition (ECCE), Baltimore, MD, USA, 29 September–3 October 2019; pp. 6041–6045.
19. Zhang, J.P.; Zhao, C.Y. Research on Circulation Current and Suppressing Strategy of Modular Multilevel Converter. *Trans. China Electrotech. Soc.* **2013**, *28*, 328–336.
20. Konstantinou, G.; Pou, J.; Ceballos, S. Control of Circulating Currents in Modular Multilevel Converters Through Redundant Voltage Levels. *IEEE Trans. Power Electron.* **2016**, *31*, 7761–7769. [[CrossRef](#)]
21. Chakraborty, R.; Dey, A. Circulating Current Control of Modular Multilevel Converter With Reduced Conduction Loss for Medium-Voltage Applications. *IEEE Trans. Power Electron.* **2021**, *68*, 9014–9023. [[CrossRef](#)]
22. Xiong, X.; Wang, X.; Liu, D. Common-mode insertion indices compensation with capacitor voltages feedforward to suppress circulating current of MMCs. *CPSS Trans. Power Electron. Appl.* **2020**, *5*, 103–113. [[CrossRef](#)]
23. Reddy, G.A.; Shukla, A. Arm-Current-Sensorless Circulating Current Control of MMC. *IEEE Trans. Ind. Appl.* **2022**, *58*, 444–456. [[CrossRef](#)]
24. Ilves, K.; Antonopoulos, A.; Norrga, S. Steady-State Analysis of Interaction Between Harmonic Components of Arm and Line Quantities of Modular Multilevel Converters. *IEEE Trans. Power Electron.* **2011**, *27*, 57–68. [[CrossRef](#)]
25. Pou, J.; Ceballos, S.; Konstantinou, G. Circulating Current Injection Methods Based on Instantaneous Information for the Modular Multilevel Converter. *IEEE Trans. Ind. Electron.* **2015**, *62*, 777–788. [[CrossRef](#)]
26. Li, B.; Li, R.; Williams, B.W. Energy transfer analysis for capacitor voltage balancing of modular multilevel converters. In Proceedings of the 2016 IEEE Transportation Electrification Conference and Expo (ITEC), Dearborn, MI, USA, 27–29 June 2016; pp. 1–6.
27. Dekka, A.; Wu, B.; Zargari, N.R. A Novel Modulation Scheme and Voltage Balancing Algorithm for Modular Multilevel Converter. *IEEE Trans. Ind. Appl.* **2016**, *52*, 432–443. [[CrossRef](#)]

Disclaimer/Publisher's Note: The statements, opinions and data contained in all publications are solely those of the individual author(s) and contributor(s) and not of MDPI and/or the editor(s). MDPI and/or the editor(s) disclaim responsibility for any injury to people or property resulting from any ideas, methods, instructions or products referred to in the content.